Elastic constants of 3-, 4- and 6-connected chiral and anti-chiral honeycombs subject to uniaxial in-plane loading

ALDERSON, Andrew, ALDERSON, K.L., ATTARD, D., EVANS, K.E., GATT, R., GRIMA, J.N., MILLER, W., RAVIRALA, N., SMITH, C.W. and ZIED, K.

Published version

ALDERSON, Andrew, ALDERSON, K.L., ATTARD, D., EVANS, K.E., GATT, R., GRIMA, J.N., MILLER, W., RAVIRALA, N., SMITH, C.W. and ZIED, K. (2010) Elastic constants of 3-, 4- and 6-connected chiral and anti-chiral honeycombs subject to uniaxial in-plane loading. Composites Science and Technology, 70 (7). 1042-1048. ISSN 0266-3538

Elastic constants of 3-, 4- and 6- connected chiral and antichiral honeycombs subject to uniaxial in-plane loading

A. Alderson[1*], K. L. Alderson[1], D. Attard[2], K. E. Evans[3], R. Gatt[2], J. N. Grima[2], W. Miller[3], N. Ravirala[1], C. W. Smith[3] and K. Zied[1]

[1] Centre for Materials Research and Innovation, University of Bolton, Deane Road, Bolton BL3 5AB, UK.

[2] Faculty of Science, University of Malta, Msida MSD 06, Malta.

[3] Department of Engineering, University of Exeter, Exeter EX4 4QF, UK.

Abstract

Finite Element models are developed for the in-plane linear elastic constants of a family of honeycombs comprising arrays of cylinders connected by ligaments. Honeycombs having cylinders with 3, 4 and 6 ligaments attached to them are considered, with two possible configurations explored for each of the 3- (trichiral and anti-trichiral) and 4- (tetrachiral and anti-tetrachiral) connected systems. Honeycombs for each configuration have been manufactured using rapid prototyping and subsequently characterised for mechanical properties through in-plane uniaxial loading to verify the models. An interesting consequence of the family of 'chiral' honeycombs presented here is the ability to produce negative Poisson's ratio (auxetic) response. The deformation mechanisms responsible for auxetic functionality in such honeycombs are discussed.

Keywords: A. Smart materials; B. Mechanical properties; C. Deformation; C. Elastic properties; C. Finite element analysis (FEA)

*** Corresponding author**: Tel: +44 (0)1204 903513; Fax: +44 (0)1204 399074; Email: A.Alderson@bolton.ac.uk

1. Introduction

Cellular honeycomb structures are widely used in a variety of engineering applications, such as strong and light-weight sandwich panel composites incorporating honeycomb core materials in aerospace and automotive sectors. An interesting class of honeycombs is those which exhibit the novel property of negative Poisson's ratio behaviour [1]. Materials that show this effect are known as *auxetic* materials [2] and can have enhancements in a range of physical properties [3,4]. For example, auxetic honeycombs undergo synclastic (domed) curvature when subject to out-of-plane bending [3], which is significant in applications for curved sandwich panels, such as aircraft nose cones [5]. Auxetic honeycombs have also been reported to have potential in radomes having optimised mechanical and dielectric properties [6], and in adaptive and deployable structures [7].

An example of an auxetic in honeycomb is the chiral honeycomb [8,9] shown in Fig. 1a, comprising of an array of circular cross-section cylinders of equal radius interconnected by ligaments of equal length, the ends of which are attached tangentially to the nodes. For the purposes of this paper, we consider a 2D chiral system is one which displays a lack of mirror symmetry. The 2D system in Fig. 1a is a simplified version of a structure considered in ref [10] and is chiral since it can be either left-handed or right-handed, the two alternatives being non-superimposable mirror images of each other. Each node has six ligaments connected to it, giving this particular honeycomb a hexagonal symmetry. We, therefore, call this system a hexachiral honeycomb. The hexachiral honeycomb has been found to display in-plane mechanical isotropy with Poisson's ratio equal to -1 [9], and also enhanced out-of-plane buckling strength (due to the cylinders) [11] and enhanced out-of-plane shear resistance [12].

In this paper we report an investigation into the fabrication and modelling of an extended range of novel cylinder-ligament ('chiral') honeycomb structures, with potential for implementation in innovative smart and advanced sandwich structures.

2. Chiral honeycomb geometries

The chiral honeycombs considered in this paper are shown in Fig. 1. In addition to the hexachiral honeycomb having 6 ligaments connected to each node (Fig. 1a), honeycombs having 3 (Figs. 1b and 1c) and 4 (Figs. 1d and 1e) ligaments tangentially attached to each node were developed. Attaching adjacent nodes on opposite sides of the connecting ligament produces the trichiral and tetrachiral honeycombs (Figs. 1b and 1d), whereas attaching the nodes on the same side of the connecting ligament creates the anti-trichiral and anti-tetrachiral honeycombs (Figs. 1c and 1e) [13]. The term 'anti-chiral' defines systems containing nearest-neighbouring nodes of opposite chirality.

The circular nodes have radius r, the ligaments have length L, and the nodes and ligaments have common wall thickness t and depth d (Figure 2a). We define three dimensionless parameters: $\alpha = L/r$, $\beta = t/r$ and $\gamma = d/r$.

3. Finite Element model development

3.1 Tetrachiral and Anti-tetrachiral honeycombs

Finite Element (FE) modelling was carried out using the Abaqus software package (Version 6.7-1). 8 node quadratic elements, linear geometry and small displacements were employed. Quadratic elements reduce computational time since a lower mesh density can be achieved than with linear elements. We were not able to employ classical mixed quadrilateral and triangular elements in Abaqus when quadratic elements were used. Element type was found to make no difference to the results for small deformations and so solely triangular elements were employed. Figs. 2a and 2b show the representative volume elements (RVEs) used for the tetrachiral and anti-tetrachiral honeycombs, respectively. For the tetrachiral honeycomb, a protruding ligament mid-point was constrained to move along a line passing through the centre of the circular node and the opposite ligament mid-point as shown in Fig. 2a. This constrains the deformations of the ligament mid-points to be along that line (there is no constraint on the geometric coordinates). In the case of the anti-tetrachiral honeycomb, the end faces

of the protruding half ribs were constrained to remain parallel to their neighbour, thus constraining the deformations of the neighbouring ligament mid-points to move along the edge of the RVE on which they are located.

3.2 Trichiral and Anti-trichiral honeycombs

The in-plane mechanical properties were modelled using the ANSYS FE package, version 10.0. Solely triangular PLANE2 (linear elastic, solid) elements were employed for consistency with the Abaqus FE simulations in the preceding sub-section. Figure 3 shows the boundary conditions applied to the RVEs for the trichiral and anti-trichiral models. The RVE edges pass through ligament mid-points. Equivalent ligament mid-points on opposing vertical RVE edges were coupled to maintain equivalent y coordinates, and equivalent ligament mid-points on opposing horizontal RVE edges were coupled to maintain equivalent x coordinates. This constrains the deformations of a pair of equivalent ligament mid-points to be along the line connecting them (there is no constraint on the geometric coordinates). For loading in the x-direction, forces were applied to the ligament nodes on the left-hand and right-hand edges of the RVE. For loading along y, forces were applied to the ligament nodes on the top and bottom edges.

3.3 Hexachiral honeycombs

A 2D array of 9×9 cells was modelled using the Abaqus software.

3.4 Prediction of Poisson's ratios and Young's moduli

The strain in the i (= x or y) direction (ε_i) was calculated from the relative displacement in the i direction of pairs of ligament nodes having the same j (= y or x) coordinate. The Poisson's ratios were calculated from

$$\nu_{ij} = -\frac{\varepsilon_j}{\varepsilon_i} \qquad (1)$$

where i is the direction of uniaxial compression.

Total stress (σ) was given by the sum of the nodal reaction forces on the edge to which compression was applied divided by the cross sectional area of the respective edge. The Young's moduli were then calculated using

$$E_i = \frac{\sigma_i}{\varepsilon_i} \tag{2}$$

4. Experimental

4.1 Honeycomb fabrication

Samples were manufactured using selective laser sintering Rapid Prototyping (RP) of Nylon powder (Duraform). Dimensions were accurate to +/- 0.1 mm. Trichiral (Tri 1), anti-trichiral (Anti Tri 1), tetrachiral (Tet 1), anti-tetrachiral (Anti-Tet 1) and hexachiral (Hex 1) honeycombs were made having r = 5mm, L = 25mm, t = 1.5mm and d = 25mm (i.e. $\alpha = \gamma = 5$, $\beta = 0.3$). A second anti-trichiral (Anti Tri 2) honeycomb was also fabricated: r = 5mm, L = 20mm, t = 2mm and d = 25mm ($\alpha = 4$, $\beta = 0.4$ and $\gamma = 5$).

4.2 Mechanical properties characterisation

The honeycombs were tested in compression in a universal testing machine (hexa-, tetra- and anti-tetrachirals: Instron 8872; tri- and anti-trichirals: Instron 3369). Videoextensometry (MESSPHYSIK ME 46 videoextensometer [14]) was also employed to optically measure axial and transverse displacements by tracking fiducial markers located on the samples along and transverse to the loading direction. Samples were tested up to typically 1 or 2% applied compressive strain. Due to symmetry the hexachiral, tetrachiral and anti-tetrachiral honeycombs were only tested along one direction. The trichiral and anti-trichiral honeycombs were tested in each of the x and y directions. Testing of the material forming the ligaments and cylinders gave a compressive modulus of E_s = 1.6GPa.

5. Results

5.1 Young's moduli

Figure 4 shows linear stress-strain response up to 1% compressive strain for each honeycomb (the response at low strain (<0.1%) corresponds to the samples conforming to the loading surfaces and taking up of any slack in the testing set-up). The slopes of the curves increase with increasing ligament number, indicating an increase in the Young's moduli, although the increase is not simply proportional to ligament number. The antichiral honeycombs have lower moduli than their chiral counterparts having the same ligament coordination number.

Young's modulus was calculated for each system by taking the slope of the best fit straight line to the data in Figure 4. Table 1 contains the experimental and FE model (using E_s = 1.6GPa) Young's moduli. Reasonable agreement is achieved, with the experimental data generally showing a slight increase over the FE model prediction. The FE model predicts the same dependency of Young's modulus on ligament number and chiral versus antichiral geometry as observed experimentally. Figure 5 shows the FE model Young's moduli as a function of β. Young's modulus increases with increasing ligament thickness (increasing β).

Figure 6 shows the Young's modulus versus α trends predicted by the FE models. In the models, $\beta = 0.10$ for the hexachiral, tetrachiral and anti-tetrachiral honeycombs, and $\beta = 0.05$ for the trichiral and anti-trichiral honeycombs. $\gamma = 5$ was used throughout. Young's modulus decreases with increasing ligament length (α).

The FE simulations predict very similar moduli in the x and y directions for each of the trichiral and anti-trichiral honeycombs.

5.2 Poisson's ratios

Poisson's ratio was determined from the negative of the slope of the transverse strain vs axial strain data for each honeycomb which was typically subject to several compression cycles. The compression tests were found to lead to repeatable strain

response. Figure 7 shows the compressive transverse strain versus compressive axial strain for the 5th compression test on the hexachiral honeycomb, by way of example. The slope of this curve is 0.80, giving a Poisson's ratio of -0.80. Analysis of all 6 compression cycles in this case yielded an average Poisson's ratio of -0.81±0.03.

Table 1 also compares the experimental and FE model Poisson's ratios. In general excellent agreement is achieved between experiment and theory for Poisson's ratio. The main exception is for the tetrachiral honeycomb where the experimental measurement of -0.26 is of significantly lower magnitude than the FE prediction of -0.83. The experimental data showed a kink in the transverse strain data for this honeycomb and so it is likely experimental error accounts for this discrepancy.

The FE model Poisson's ratio vs β predictions are shown in Figure 8. The 6- and 4-coordinated honeycombs are predicted to have large negative Poisson's ratios for all values of β in Figure 8, having a value close to -1 at low β, before eventually decreasing slightly in magnitude at higher β values. This is most pronounced for the hexachiral system (Poisson's ratio = -0.58 at $\beta = 0.4$).

Positive Poisson's ratios are predicted for the trichiral honeycomb for all values of β in Figure 8. A slight increase in ν with increasing β is predicted. The FE model also predicts increasing Poisson's ratios with increasing β for the anti-trichiral system, but in this system a transition from negative Poisson's ratio at low β (thin ligament) to positive Poisson's ratio at high β (thick ligament) occurs.

Figure 9 plots the predicted Poisson's ratios as a function of α ($\beta = 0.10$ for the hexachiral, tetrachiral and anti-tetrachiral honeycombs; $\beta = 0.05$ for the trichiral and anti-trichiral honeycombs; $\gamma = 5$ for all honeycombs). The 6- and 4-coordinated honeycombs retain a negative Poisson's ratio close to -1 for all values of α, indicating the Poisson's ratio is largely insensitive to the ligament length-to-cylinder radius ratio. The trichiral and anti-trichiral honeycombs are both predicted to increase Poisson's ratio with increasing α. The trichiral honeycomb is predicted to have a positive Poisson's

ratio for all values of α investigated, whereas the model predicts the anti-trichiral will undergo a transition from negative Poisson's ratio at low α (short ligament limit) to positive Poisson's ratio at high α (long ligament limit).

The second anti-trichiral honeycomb ('Anti Tri 2') contains a smaller ligament length to cylinder radius ratio ($\alpha = 4$) than 'Anti Tri 1' ($\alpha = 5$) and was produced to confirm the short ligament limit auxetic response of the anti-trichiral system. Based on the observation that the Poisson's ratio is predicted to be the same in the x and y direction for this system (Figs. 8 and 9), the model was used to predict the Poisson's ratio response for 'Anti Tri 2' subject to loading in the x direction only. The experimental values of $\nu_{xy} = -0.11$ and $\nu_{yx} = -0.10$ confirm the x and y directed Poisson's ratios are similar and both negative as predicted for the 'short ligament' anti-trichiral honeycomb. The FE model prediction of -0.06 is in reasonable agreement with experiment (Table 1).

5.3 Deformation mechanisms

The chiral and anti-chiral honeycombs deform predominantly by a combination of cylinder rotation and ligament bending. For example, Figure 10a shows the local cylinder-ligament structure of the anti-trichiral honeycomb predicted from the FE model before and after deformation. The applied compressive load generates a torque on the cylinders such that they undergo in-plane rotation. This rotation induces a moment on the ligaments connected to each cylinder causing them to bend. In the case of the anti-trichiral honeycomb the bending of the ligaments forms a half-wave ligament shape. The ligaments of the anti-tetrachiral honeycomb were also found to form a half-wave shape under in-plane uniaxial loading.

On the other hand, the 'off-axis' ligaments in the trichiral system undergo flexure into a full-wave shape (Figure 10b), rather than the half-wave shape observed in the anti-trichiral system. The flexure of Figure 10b is again a consequence of the

cylinder rotation effect due to the generation of a torque on the cylinders by an applied load. However, it is noticeable that the cylinder rotation is significantly lower than that observed in the anti-trichiral system, and that ligament flexure also occurs due to orientation of the off-axis ligament itself. Full-wave ligament shape was also found for the hexachiral and tetrachiral systems under in-plane uniaxial loading.

6. Discussion

In this paper we have performed a systematic study of 2-D periodic honeycombs made up of rigid circular nodes linked to each other by ligaments that are tangentially connected to the nodes. The chiral systems are characterised by cylinders attached to opposite sides of the connecting ligament so that the system can be either left-handed or right-handed, the two being non-superimposable mirror images of each other. Such chiral systems can only be constructed from repeat units having a 3-, 4- or 6- fold symmetry. Connecting the cylinders on the same side of the ligament leads to the anti-chiral systems. These systems, which are racemic, have an equal number of left- and right- handed repeat units and therefore the unit cell must contain an even number of nodes. This only allows for anti-trichirals and anti-tetrachirals to exist.

We have found that the modulus of these honeycombs decreases as the number of ligaments attached to each cylinder decreases. This is intuitive since it is clear that the trichiral system, for example, is a more open, less constrained and therefore more compliant structure than the hexachiral system which contains more connecting ligaments. The deformation modes observed in these structures have been found to be simultaneous flexure of off-axis ligaments, rotation of cylinder nodes and flexing of ligaments as a result of cylinder node rotation. In the latter mechanism, the ligaments form a half-wave shape in the anti-chiral systems (e.g. Figure 10a) and a full-wave shape in the chiral systems (e.g. Figure 10b). The formation of a full wave is a higher energy deformation mode than that of a half wave [1] and explains why the chiral

structures have a higher in-plane compressive modulus than the antichiral structures for any given ligament number (Table 1 and Figures 5 and 6).

Contrary to the 6- and 4-connected systems, which are auxetic, the trichiral honeycomb possesses positive in-plane Poisson's ratios. The anti-trichiral honeycomb is auxetic in the short ligament limit but possesses positive Poisson's ratios in the long ligament limit. The observed and predicted Poisson's ratio response of the trichiral and anti-trichiral systems can be understood qualitatively by considering the effects of the competing mechanisms of ligament flexure due to cylinder rotation and direct flexure of the off-axis ligaments in response to an applied load.

In the trichiral honeycomb, direct flexing of the off-axis ligaments and ligament flexing due to cylinder rotation both lead to a full-wave ligament shape (Figure 10b). The effects are additive, leading to full-wave ligament shape formation being the dominant mechanism in both the short and long ligament limits. The trichiral honeycomb cell structure reduces to the regular hexagonal cell shape as $r \rightarrow 0$. Full-wave flexure of ligaments in a regular hexagonal cell structure is known to lead to positive Poisson's ratio response [1], thus explaining the positive Poisson's ratios observed and predicted for the trichiral system over all ranges of α (ligament length-to-cylinder radius ratio) in Figure 9.

In the case of the anti-trichiral honeycomb the flexing of the ligaments due to cylinder rotation causes half-wave ligament shape formation (Figure 10a), which results in a shortening of the cylinder-cylinder distance and a tendency to contract the structure in both in-plane principal directions. Cylinder rotation is, therefore, a mechanism for auxetic behaviour in the anti-trichiral honeycomb. As for the trichiral system, direct flexing of off-axis ligaments leads to full-wave ligament shape formation and positive Poisson's ratio response (the anti-trichiral honeycomb also reduces to a regular hexagonal honeycomb as $r \rightarrow 0$). Hence in the short ligament limit the anti-trichiral system displays auxetic behaviour due to cylinder rotation (half-wave ligament shape)

dominating the deformation response (Figure 9). On the other hand, in the long ligament limit, off-axis ligament full-wave flexure dominates leading to positive Poisson's ratios.

With the exception of ν_{xy} and ν_{yx} for the trichiral honeycomb, the trichiral and anti-trichiral systems appear to demonstrate equivalence in the *x*- and *y*- directed elastic properties (within the uncertainties inherent in the modelling and experimental approaches employed). The slight deviation from equality of ν_{xy} and ν_{yx} for the trichiral honeycomb (Figs. 8 and 9) is unexpected and possibly indicates the RVE with periodic boundary conditions approach applies too much constraint on the complex multiple deformation mechanism system.

Identification of the deformation mechanisms enables analytical expressions to be developed for the Poisson's ratios and Young's moduli of the honeycombs considered in this paper. This has already been reported for the hexachiral system assuming ligament bending [9]:

$$\nu_{xy} = \nu_{yx} = -1 \tag{3}$$

and

$$E_x = E_y = E_s \sqrt{3} \frac{t^3}{lr^2} \tag{4}$$

It is beyond the scope of this paper to derive analytical expressions for all other chiral and antichiral honeycombs considered here. These will be reported elsewhere, along with detailed analysis of the analytical model predictions. Since expressions exist for the hexachiral system [9], and we have a qualitative understanding of the 3-coordinated systems (see above), we derive here analytical expressions for one of the 4-coordinated systems (the anti-tetrachiral honeycomb) to illustrate how the micromechanics determined from the FE models can be developed into analytical form.

As a first approximation, we assume the cylinders are perfectly rigid and that only small ligament deformations occur so that conventional beam theory is applicable. Anti-tetrachiral systems are described here by a unit cell containing four cylinders and

eight whole ligaments as shown in Figure 10c. As noted above, when such a system is subjected to an external compressive stress acting along the x direction, adjacent cylinders rotate in opposite directions, causing half-wave bending of the ligaments.

For systems in which the ligament thickness is comparable to the cylinder radius, it is necessary to take into account the fact that the neutral axis of the ligament does not coincide with the cylinder outer surface, and also that a relatively large volume of material of the cylinder significantly constrains a small region of the ligament close to the cylinder (shaded regions in Figs. 10d and 10e). We therefore consider an effective flexural length l_{eff} of the beam rather than its actual length *l*. Referring to Fig. 10d, to a first approximation the effective length is

$$l_{eff} = l - 2\mathrm{AB} = l - 2\sqrt{r^2 - (r-t)^2} = l - 2\sqrt{2rt - t^2} \tag{5}$$

In the case of low strain deformation, the distance between two cylinders is

$$R = l - 2(r - t/2)\cos(\zeta) \tag{6}$$

where ζ is the angle between a line joining the centre of the cylinder to the ligament-cylinder junction and a line joining two such junctions that the ligament makes with two adjacent cylinders (Figure 10d).

Upon loading, the angle ζ changes by an angle ϕ, with a concomitant rotation of the cylinders by an equal angle ϕ. From geometric considerations, it follows that the change in distance *R* in the small strain limit ($\zeta \to 90^\circ$) between two connected cylinders is

$$dR = 2(r - t/2)\sin(\zeta)\, d\zeta = 2(r - t/2)\phi \tag{7}$$

The engineering strains ε_i in both the x and y directions are

$$\varepsilon_i = \frac{dR}{R} = \frac{2(r - t/2)\phi}{l} \tag{8}$$

and thus the Poisson's ratios for the anti-tetrachiral honeycomb are

$$\nu_{xy} = \left(\nu_{yx}\right)^{-1} = -\frac{\varepsilon_y}{\varepsilon_x} = -1 \tag{9}$$

The Young's moduli can be found from an energy approach by equating the strain energy due to an incrementally small strain ε_i in the i direction to the energy W_{rib} stored in each of the eight bent ribs of each unit cell

$$U = \frac{1}{2} E_i \varepsilon_i^2 = \frac{8}{V} W_{rib} \tag{10}$$

where V is the volume of the unit cell ($V = 4l^2 z$ and z is the unit-cell depth equal to the ligament and cylinder depth d). From standard beam theory, the energy stored in a single deformed ligament (beam) which is symmetrically bent by two equal and opposing moments M acting on each 'edge' of the ligament resulting in the angular deflection φ is

$$W_{rib} = 2\int_0^{\varphi} M d\varphi \tag{11}$$

where, for a ligament of effective length l_{eff}, $\varphi = {Ml_{eff}}/{2E_s I}$ and I ($= {zt^3}/{12}$) is the second moment of area. The energy stored in each rib for a given ϕ is then

$$W_{rib} = \frac{4E_s I}{l_{eff}} \int_0^{\varphi} \varphi d\varphi = \frac{2E_s I}{l_{eff}} \varphi^2 = \frac{E_s z t^3 l^2}{24 l_{eff} \left(r - t/2\right)^2} \varepsilon_i^2 \tag{12}$$

and from equations (10) and (12), the Young's moduli for the anti-tetrachiral system are

$$E_x = E_y = \frac{E_s t^3}{6 l_{eff} \left(r - t/2\right)^2} \tag{13}$$

We note that the Young's moduli expressions for both the hexachiral and anti-tetrachiral systems (equations (4) and (13)) contain a t^3 term in the numerator, thus explaining the increase in modulus with increasing β (= t/r) from the FE models in Figure 5. Similarly, the decrease in modulus with increasing α (= l/r) in the FE models (Figure 6) is explained by the inverse dependency on ligament length in equations (4) and (13).

Employing E_s = 1.6GPa and the ligament and cylinder dimensions contained for the hexachiral and anti-tetrachiral honeycombs ('Hex 1' and 'Anti Tet 1'), in equations

(4) and (13), respectively, yields predictions for the Young's moduli of 14.96MPa (hexachiral) and 2.79MPa (anti-tetrachiral), in excellent agreement with experiment and FE model predictions (Table 1). The analytical model predictions of $\nu_{xy} = \nu_{yx} = -1$ for both systems are close to the experimental and FE model values in Table 1.

Poisson's ratio is less sensitive to small (i.e. a few percent) variations in ligament dimensions and intrinsic ligament modulus than Young's modulus (e.g. Figs. 5, 6, 8 and 9, and equations (3), (4), (9) and (13)). Consequently, any slight deviation of the experimental geometrical and ligament modulus parameters from those employed in the models will lead to greater discrepancy in the predicted and experimental Young's modulus than for Poisson's ratio (Table 1). Additionally, since Poisson's ratio is by definition a ratio of two strains (equation (1)), any systematic experimental error in the measurement of strain will cancel out when measuring Poisson's ratio, whereas it will persist in tandem with any error in stress measurement when evaluating Young's modulus (equation (2)), again tending to greater discrepancy between theory and experiment for Young's modulus.

The 3-, 4- and 6- connectivity systems investigated in this paper have been modelled under conditions replicating the uniaxial in-plane compression test, i.e. no in-plane shear strain. Under such conditions, it is clear that the honeycombs behave effectively as rigid cylinders connected by flexible beams or plates. This aids the design process considerably since they can be modelled via relatively simple beam mechanics approaches (e.g. [1,9,13]) when optimising honeycombs for specific applications. It should be noted that for the chiral systems, and in contrast to their anti-chiral versions, there is an in-plane coupling between on-axis deformations and shearing deformations. In the situation where shear strains are allowed to be non-zero, then an in-plane shear develops in the chiral systems when under an applied on-axis uniaxial stress, indicating such systems may exhibit non-classical Cosserat or micropolar type elasticity [9]. To accurately model the chiral systems under such conditions will require the use of a

homogenised micropolar type element or entire discrete honeycomb structures with appropriate boundary conditions to be employed.

7. Conclusions

In conclusion, the in-plane Young's moduli and Poisson's ratios of hexachiral, tetrachiral, anti-tetrachiral, trichiral and anti-trichiral rapid prototyped honeycombs have been measured and found to be in good agreement with FE model predictions. The FE models have enabled the major deformation mechanisms to be identified, comprising rotation of cylinders, flexing of ligaments due to cylinder rotation, and direct flexing of ligaments oriented at an angle to the applied load. The FE model mechanical property dependencies on ligament and cylinder dimensions can be confirmed through the development of analytical expressions based on the identified deformation mechanisms. The Young's moduli increase with increasing ligament coordination number. The 4- and 6- connected honeycombs are auxetic, with values of Poisson's ratio close to -1. The trichiral system always displays positive Poisson's ratio response, whereas the anti-trichiral system displays negative Poisson's ratios in the short ligament limit and positive Poisson ratios in the long ligament limit.

Acknowledgements. This work has been performed as part of the European Union 6th Framework Programme STREP project NMP3-CT-2005-013641 - CHISMACOMB.

References

1. Gibson LJ, Ashby MF. Cellular solids, Structure and Properties. Cambridge University Press, Cambridge, second edition, 1997.

2. Evans KE, Nkansah MA, Hutchinson IJ, Rogers SC. Molecular Network Design, Nature 1991;353:124.

3. Lakes R. Foam structures with a negative Poisson's ratio. Science 1987;235:1038-1040.

4. Evans KE, Alderson A. Auxetic Materials: Functional Materials and Structures from Lateral Thinking!, Adv. Mater. 2000;12(9):617-624.

5. Alderson A, Alderson KL. Auxetic Materials. Proc. Inst. Mech. Eng., Part G, J. Aero. Eng. 2007;221:565-575.

6. Scarpa F, Burriesci G, Smith FC, Chambers B. Mechanical and dielectric properties of auxetic honeycomb structures. Aer. J. 2003;107:175-183.

7. Hassan MR, Scarpa F, Mohammed NA, Ancrenaz Y. Conventional and auxetic SMA cellular structures. ASME Aerosp. Div. Publ. AD, 70 AD. 2005. p. 451-456.

8. Lakes R. Deformation mechanisms in negative Poisson ratio materials - Structural aspects, J. Mater. Sci. 1991;26 (9):2287-2292.

9. Prall D, Lakes R. Properties of a chiral honeycomb with Poisson's ratio –1. Int. J. Mech. Sci. 1996;39:305-314.

10. Wojciechowski KW. Two-dimensional isotropic system with a negative Poisson ratio, Physics Letters A 1989;137:60-65.

11. Spadoni A, Ruzzene M, Scarpa F. Global and local linear buckling behaviour of a chiral cellular structure. Physica Status Solidi (b) 2005;242(3):695–709.

12. Lew TL, Spadoni A, Scarpa F, Ruzzene M. Chiral hexagonal cellular sandwich structure: A vibroacoustic assessment. Proceedings of SPIE 2005;5760:559-568.

13. Grima JN. New Auxetic Materials, PhD thesis, Exeter University, 2000.

14. Messphysik videoextensometer package, Messphysik, Laborgerrite Ges. M.B.H., Fürstenfeill, Austria.

FIGURES

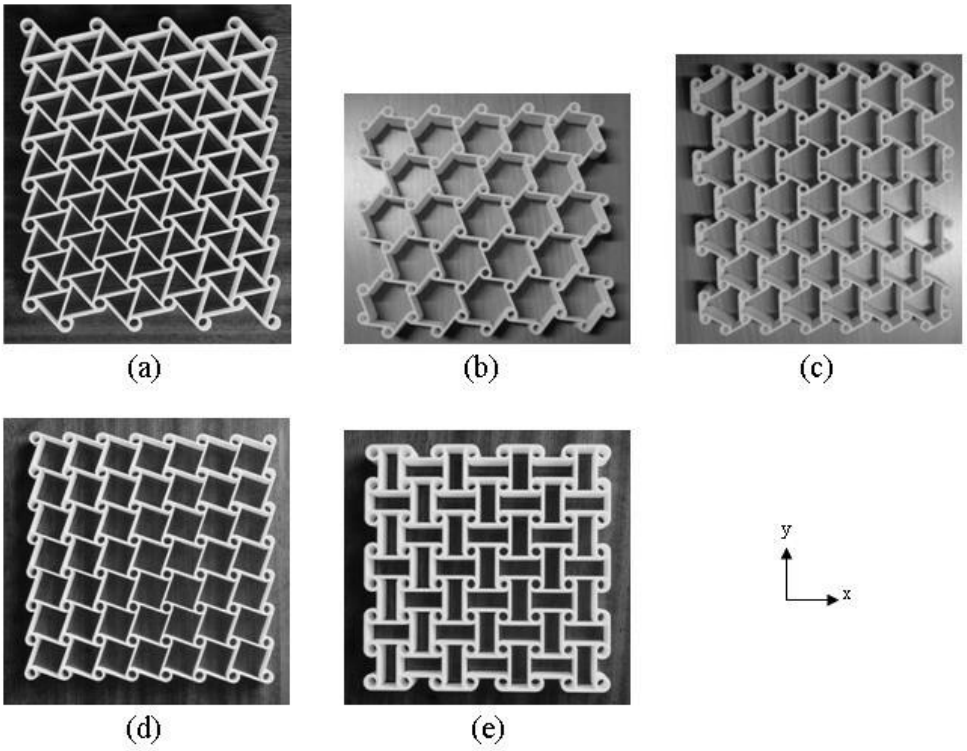

Fig. 1 Rapid prototype chiral honeycombs investigated in this study: (a) Hexachiral; (b) Trichiral; (c) Anti-trichiral; (d) Tetrachiral; (e) Anti-tetrachiral.

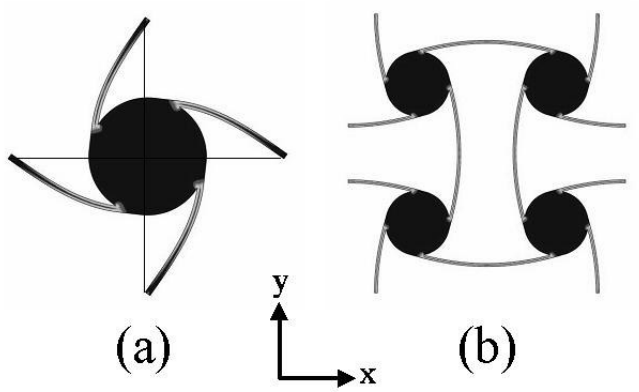

Fig. 2 Boundary conditions and RVEs used in the FE simulations for the (a) tetrachiral and (b) anti-tetrachiral honeycombs.

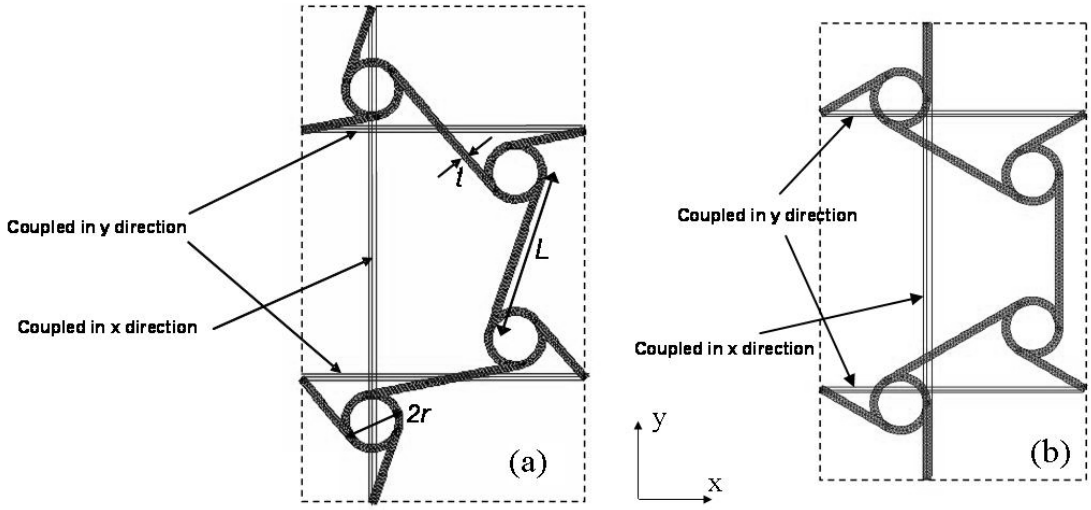

Fig. 3 Unit-cell representations showing periodic boundary conditions for (a) the trichiral honeycomb and (b) the anti-trichiral honeycomb. Geometrical parameters are also indicated in (a).

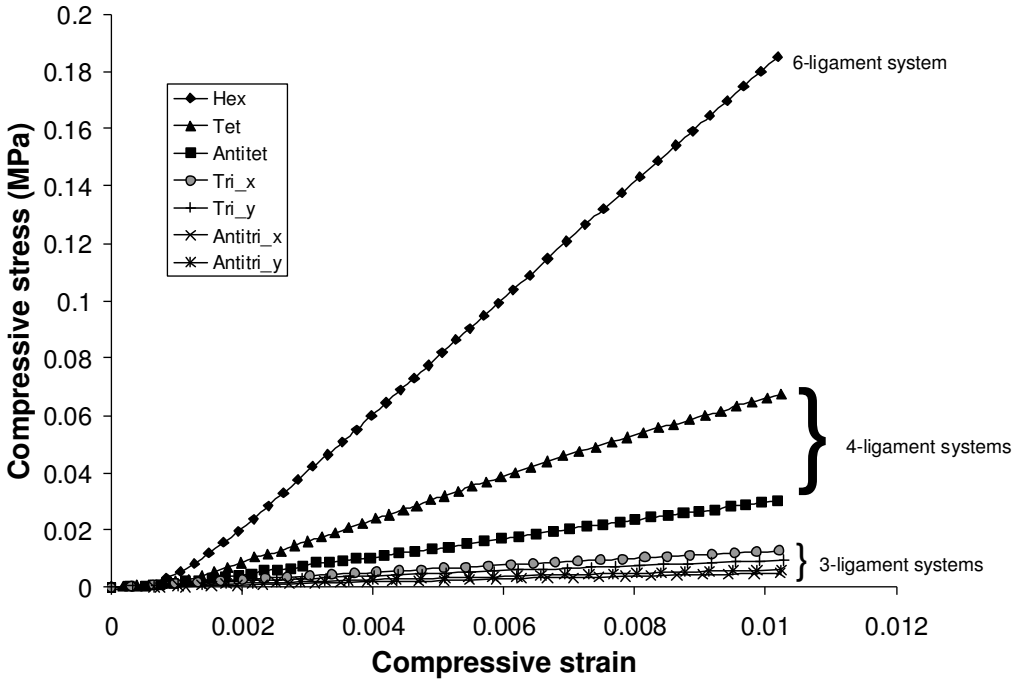

Fig. 4 Experimental compressive stress-strain data for hexachiral, tetrachiral, anti-tetrachiral, trichiral (x and y loaded) and anti-trichiral (x and y loaded) honeycombs.

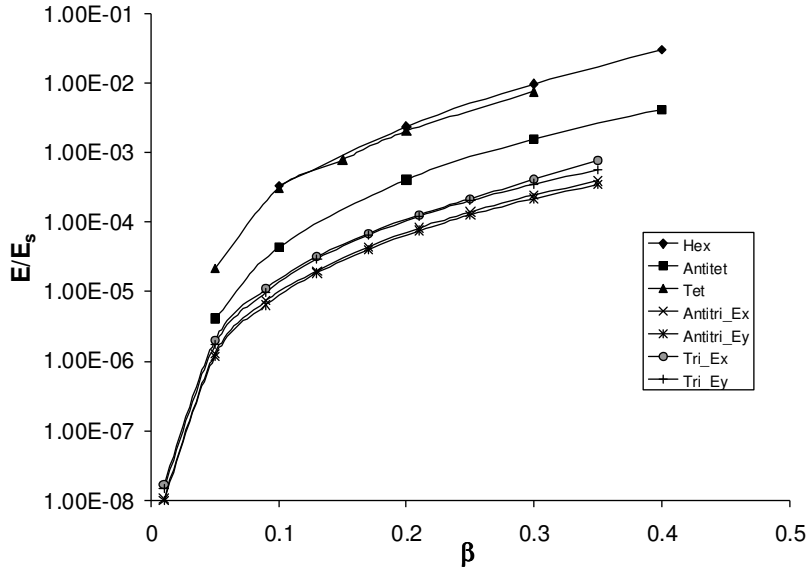

Fig. 5 FE model predictions of Young's modulus (E/E_s) as a function of β (= t/r) for the hexachiral (diamond), anti-tetrachiral (squares), tetrachiral (triangles), anti-trichiral (crosses – x direction; stars – y direction); and trichiral (circles – x direction; plus signs – y direction) honeycombs. FE model simulations employed α (= L/r) = γ (= d/r) = 5 in all cases.

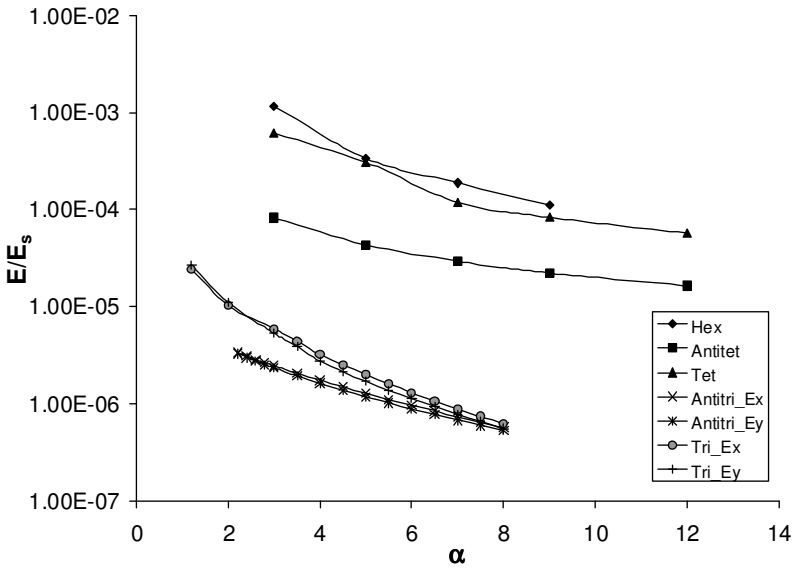

Fig. 6 FE model predictions of Young's modulus (E/E_s) vs α (= L/r). Symbols as for Fig. 5. β = 0.05 for the trichiral and anti-trichiral honeycombs; β = 0.10 for the hexachiral, tetrachiral and anti-tetrachiral honeycombs; γ = 5 for all cases.

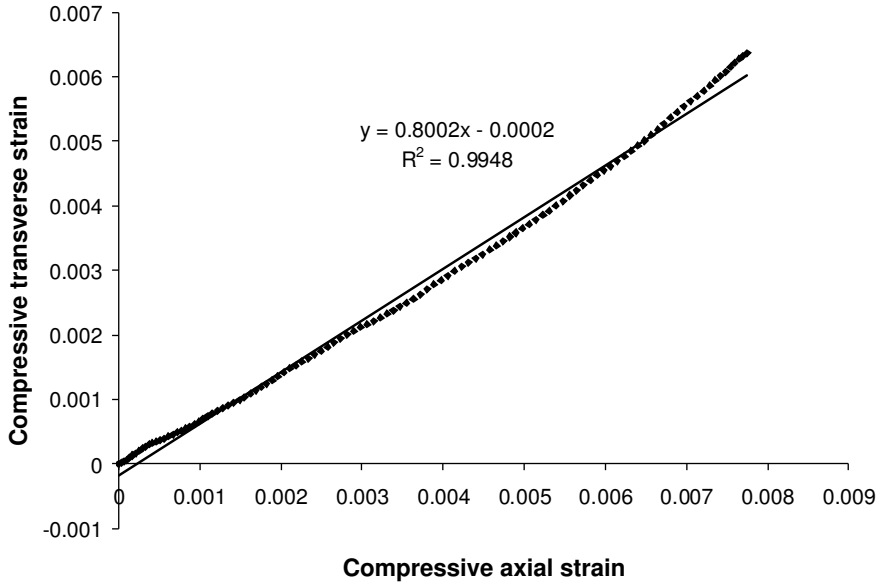

Fig. 7 Experimental compressive transverse strain vs compressive axial strain data for the hexachiral honeycomb (5th compression test).

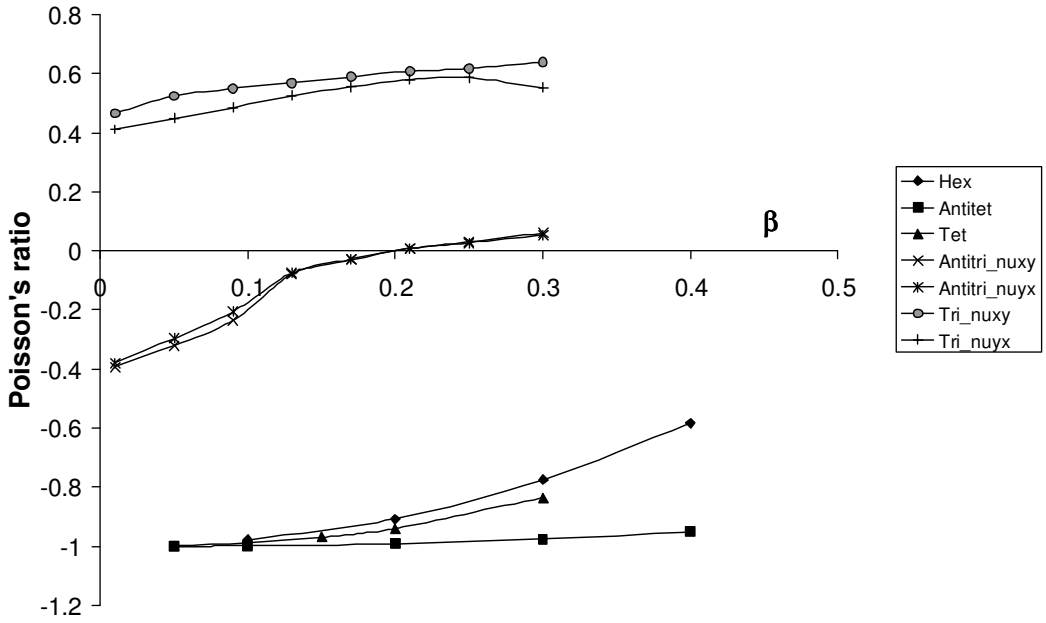

Fig. 8 FE model predictions of Poisson's ratio as a function of β. Symbols as for Fig. 5. $\alpha = \gamma = 5$ in all cases.

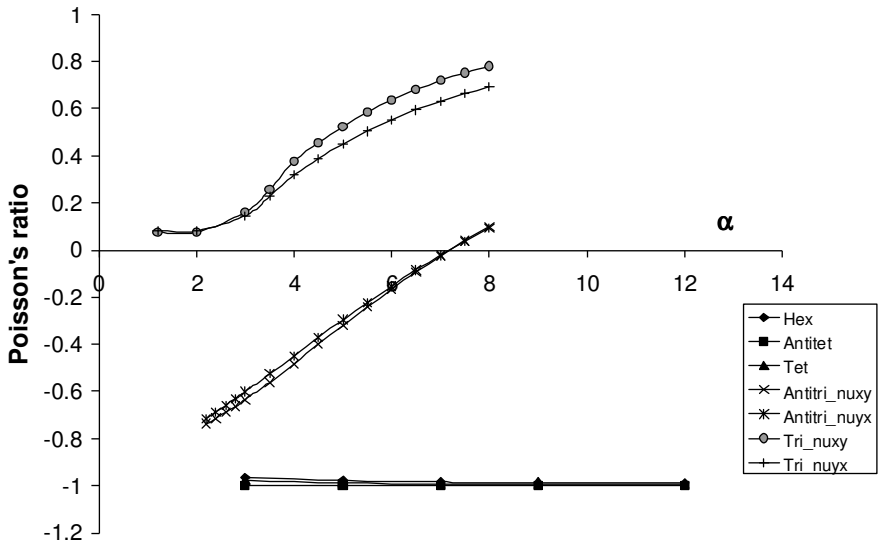

Fig. 9 FE model predictions of Poisson's ratio as a function of α. Symbols as for Fig. 5. β = 0.05 for the trichiral and anti-trichiral honeycombs; β = 0.10 for the hexachiral, tetrachiral and anti-tetrachiral honeycombs; γ = 5 for all cases.

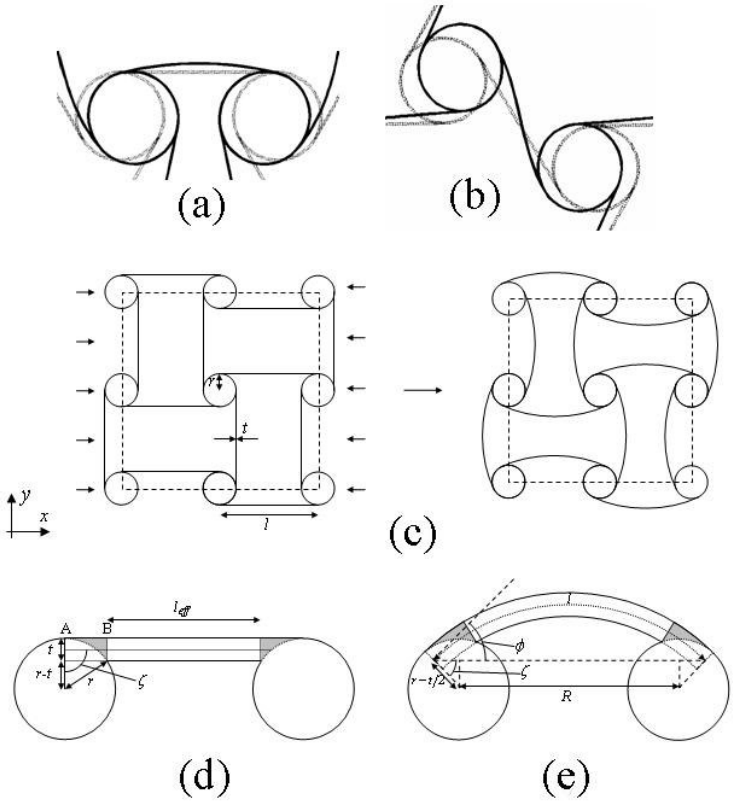

Fig. 10 (a) Cylinder rotation and half-wave flexing of ligaments in the anti-trichiral honeycomb; (b) full-wave flexing of ligaments in the trichiral honeycomb; (c)-(e) ligament flexing in the anti-tetrachiral system.

Table 1: Experimental and FE model in-plane elastic constants (Young's moduli and Poisson's ratios)

	Hex 1	Tet 1	Anti Tet 1	Tri 1	Anti Tri 1	Anti Tri 2
Experiment						
E_x (MPa)	19.46	7.08	3.11	1.25	0.57	
E_y (MPa)	19.46	7.08	3.11	0.94	0.65	
ν_{xy}	-0.81	-0.26	-0.98	+0.69	+0.08	-0.11
ν_{yx}	-0.81	-0.26	-0.98	+0.66	+0.08	-0.10
FE model						
E_x (MPa)	15.49	12.01	2.50	0.65	0.39	
E_y (MPa)	15.49	12.01	2.50	0.57	0.35	
ν_{xy}	-0.77	-0.83	-0.98	+0.64	+0.06	-0.06
ν_{yx}	-0.77	-0.83	-0.98	+0.55	+0.05	